THE JOURNAL OF PHYSICAL CHEMISTRY A
A JOURNAL OF THE AMERICAN CHEMICAL SOCIETY

pubs.acs.org/JPCA

Article

Origin of the Second-Order Proton Catalysis of Ferriin Reduction in Belousov–Zhabotinsky Reactions: Density Functional Studies of Ferroin and Ferriin Aggregates with Outer Sphere Ligands Sulfate, Bisulfate, and Sulfuric Acid

Sara C. McCauley and Rainer Glaser*

Cite This: J. Phys. Chem. A 2022, 126, 7261–7272

Read Online

ACCESS | Metrics & More | Article Recommendations | Supporting Information

ABSTRACT: The detailed mechanisms of Belousov–Zhabotinsky oscillating reactions continue to present grand challenges, even after half a century of study. The origin of the pH dependence of the oscillation pattern had never been rigorously identified. In our recent kinetic study of one of the key Belousov–Zhabotinsky reactions, the iron-catalyzed bromate oxidation of malonic acid, compelling agreement between experiments and kinetic simulations was achieved only with the inclusion of second-order proton catalysis of the reduction of the $[Fe(phen)_3]^{3+}$ species. After exhausting all other avenues in search of an explanation of this proton catalysis, we considered the possibility that the parent iron–phenanthroline complexes could aggregate with neutral and anionic outer sphere ligands (OSLs) in the highly concentrated sulfuric acid solution, and we hypothesized that OSL protonation would increase the capacity of the aggregated complex to oxidize the organic fuel. We performed potential energy surface analyses at the SMD(APFD/6-311G*) level of complexes of the types $[Fe(phen)_3(SO_4^{2-})_m(HSO_4^-)_n(H_2SO_4)_o]^{(c-2m-n)+}$ for ferriin (c = 3) and ferroin (c = 2) aggregated with m sulfate, n bisulfate, and o sulfuric acid OSLs. We present structures of the OSL aggregates, develop a nomenclature for their description, and characterize their electronic structure. The structural chemistry provides the foundation to discuss the ferroin/ferriin redox couple with emphasis on the relationship between the vertical electron affinities of ferriin aggregates and their OSL protonation states. For proton catalysis to manifest itself, double-protonation paths that are slightly endergonic should be present, and proton affinities of aggregated OSLs allow the identification of such double-protonation chains. As a first test of our mechanistic proposal for the second-order proton catalysis of the Belousov–Zhabotinsky reaction, the results presented here provide compelling evidence in support of the importance of outer sphere ligation of the iron catalyst.

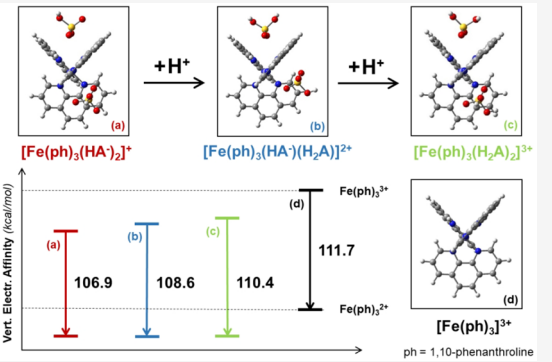

1. INTRODUCTION

Belousov–Zhabotinsky reactions have attracted much interest since their discovery almost five decades ago,[1−3] and have been at the center of the evolving field of nonlinear dynamics.[4−6] Much recent work has focused on the reaction's potential for chemical computing, artificial intelligence, and biomimetic polymers.[7−10] Belousov–Zhabotinsky reactions are the class of metal-catalyzed bromate oxidations of dicarboxylic acids. The pioneering studies involved cerium catalysis and subsequent studies employed a great variety of transition metal catalysts, including iron, manganese, copper, etc.[11] Many of the essential features of the Belousov–Zhabotinsky reaction have been described by the seminal papers by Field, Koros, and Noyes,[12] while complete reaction simulations have remained elusive. We have been interested in understanding the pH dependence of the oscillating behavior of the Belousov–Zhabotinsky reaction (BZR) with focus on iron- and/or cerium-catalyzed bromate oxidations of malonic acid. Our first contribution to studies of the BZR was the elucidation of the mechanism of disproportionation of bromous acid.[13] In parallel, we developed methods for the video analysis of the kinetics of oscillating reactions,[14,15] and we developed software for the evaluation of multiequilibria reactions using the dynamical approach.[16−18] Studies by Foersterling and Varga[19] discovered a pH dependence of this disproportionation (R4 in FKN mechanism), and the rate constant for this disproportionation was further studied by Agreda and Field.[20] Our experimental work and the associated simulations eventually shifted our focus to the pH dependence of the reduction reaction of the

Received: August 16, 2022
Revised: September 19, 2022
Published: October 4, 2022

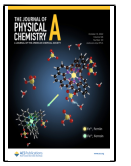

https://doi.org/10.1021/acs.jpca.2c05879
J. Phys. Chem. A 2022, 126, 7261–7272

higher oxidization state catalyst (R8 in FKN mechanism).[21] In varying the sulfuric acid concentration in the iron-catalyzed BZR, we found a strong inverse dependence of period time on acidity. In simulations of the kinetics of the iron-catalyzed reaction, strong agreement with experiment was found by including second-order proton catalysis of the electron transfer reaction (reaction R9 in ref 21, shown below) between $[Fe(phen)_3]^{3+}$ and bromomalonic acid. The goal of this paper is to investigate the possible origin of the proton dependence using *ab initio* studies of the ferriin reduction.

$$[Fe(phen)_3]^{3+} + BrMA + 2H^+ \rightarrow [Fe(phen)_3]^{2+} + Br^- + P1 + 2H^+ \quad (R9)$$

The obvious question concerns the target of the protonation. There are literature reports on the *N*-protonation of phenanthroline itself,[22] as well as reports on phenanthroline complex disintegration in acidic media over long reaction times.[22] There is no evidence of catalyst disintegration during the course of Belousov–Zhabotinsky oscillating reactions. With the $Fe(phen)_3$ core intact, we reluctantly considered the possibility of the protonation of anions aggregated with the catalyst. While counteranions have not been traditionally considered in the Belousov–Zhabotinsky reaction, there is a wealth of evidence in the crystallographic record that cationic transition metal complexes of 1,10-phenanthroline interact strongly with anionic and neutral polar outer sphere ligands (OSLs).[23−27] In fact, a number of cocrystals of phenanthrolines with anions and other neutral polar species have been reported.[28−32] In light of this evidence, it is certainly warranted to postulate that similar interactions would occur in solution, and we have chosen to consider outer sphere aggregation in our investigation into the proton dependence.

$$[Fe(phen)_3]^{3+} + 1e^- \rightarrow [Fe(phen)_3]^{2+} \quad (1a)$$

$$[Fe(phen)_3]^{3+} + Ce^{3+} \rightarrow [Fe(phen)_3]^{2+} + Ce^{4+} \quad (1b)$$

The aggregation of a cationic transition metal complex with anionic counterions provides stabilization due to electrostatic interactions, hydrogen-bonding, and van der Waals interactions. The stabilization is expected to increase with the charge of the transition metal complex, with the charge of the counterion, and with the number of counterions. As a consequence, it is reasonable to expect that the reaction energy of reduction in reaction 1a*decreases* with increasing aggregation with counterions. As a corollary, one may expect a lower driving force for the oxidation of the lower-oxidation state transition metal complex with increasing aggregation with counterions. The electron affinity of higher-oxidized species equals the ionization energy of the lower-oxidized species. In cases where the anionic counterion can be protonated, such redox reactions can be manipulated by way of their protonation state and, hence, the redox reactions become susceptible to proton catalysis. Protonation of anionic ligands leads to a higher driving force for the reduction of the higher-oxidation state complex.

We are primarily interested in the *reduction reaction* of the Fe^{3+} species and the effect of aggregation on its reduction potential. This question can be addressed based on the reduction energies computed with the optimized structures of the Fe^{3+} species, that is, the reduction is faster than the structural relaxation. Nevertheless, we studied both the optimized geometries of the Fe^{3+} and the Fe^{2+} species because the *oxidation reaction* of the Fe^{2+} species is also known to be pH dependent. Dulz and Sutin reported that the rate constant for the oxidation of tris(1,10-phenanthroline)iron(II) by cerium(IV) increases with increasing sulfuric acid concentration (reaction 1b).[33]

$$[Fe(phen)_3(SO_4^{2-})_m(HSO_4^-)_n(H_2SO_4)_o]^{(3-2m-n)+} + 1e^- \rightarrow [Fe(phen)_3](SO_4^{2-})_m(HSO_4^-)_n(H_2SO_4)_o]^{(2-2m-n)+} \quad (2)$$

Here we are reporting the results of *ab initio* studies of the redox chemistry between ferriin ($[Fe(phen)_3]^{3+}$) and ferroin ($[Fe(phen)_3]^{2+}$) depending on the aggregation with sulfate (SO_4^{2-}), bisulfate (HSO_4^-), and sulfuric acid (H_2SO_4) OSLs. Therefore, we studied the parent reaction 1a and reaction 2 with 1, 2, or 3 outer sphere ligands. At the typical pH of the Belousov–Zhabotinsky reactions, the most abundant sulfur species clearly is bisulfate, and we studied bisulfate complexes with $n = 1-3$. While the sulfate equilibrium concentration is very low in solution, sulfate might be stabilized by complex formation, and we did consider aggregates with $m = 1$. For every aggregate with sulfate and bisulfate OSLs, we also studied the respective protonated species with $o = 1-3$ sulfuric acid ligands. We will discuss the structures of ferriin and ferroin aggregates and develop a nomenclature for their description. The potential energy surface analysis was performed for the two lowest spin states of ferriin and ferroin to firmly establish that the lower spin states are preferred by both oxidation states. The spin density distributions are discussed and rationalized using MO theory. Computed ligand binding energies provide strong support of OSL aggregation in solution and fast equilibration. Adiabatic and vertical ferroin–ferriin redox energies are reported and discussed with a focus on vertical electron affinities of ferriin aggregates. We will show that OSL protonation in ferriin adducts leads to higher electron affinities. Moreover, double protonation chains are identified which might explain the second order proton catalysis of the reduction of ferriin in Belousov–Zhabotinsky reactions.

2. COMPUTATIONAL METHODS

All structures were completely optimized and vibrational frequency calculations were performed to confirm that a stationary structure had indeed been reached and to compute thermochemical parameters. We employed density functional theory[34] (DFT) and specifically the Austin–Petersson–Frisch functional with dispersion[35] (APFD). DFT has been proven to reproduce equilibrium geometries of transition metal complexes[36] and ligand substitution energies,[37] and its range of applications and limitations have been addressed in several reviews.[38−40] The APFD method was employed with the 6-311G* basis set.[41,42] The 6-311G* is the standard triple-ζ valence basis set for hydrogen and first-row atoms C, N, and O with polarization functions on the latter. The second-row atom S is described by the (631111,42111,1) contraction of the (12s,9p,1d) McClean–Chandler basis set.[43] The transition metal atom Fe is described by the (611111111,51111,311,1) contraction of the (14s,9p,5d,1f) all-electron basis set.[44,45] This theoretical level is abbreviated as APFD/6-311G*.

We are studying aggregates of $Fe(phen)_3$ complexes and employ the solvation model SMD[46] to account for bulk aqueous solvation.[47] In general, we optimized the structures and computed the thermochemistry with the inclusion of continuous solvation, and this theoretical level is referred to as

https://doi.org/10.1021/acs.jpca.2c05879
J. Phys. Chem. A 2022, 126, 7261−7272

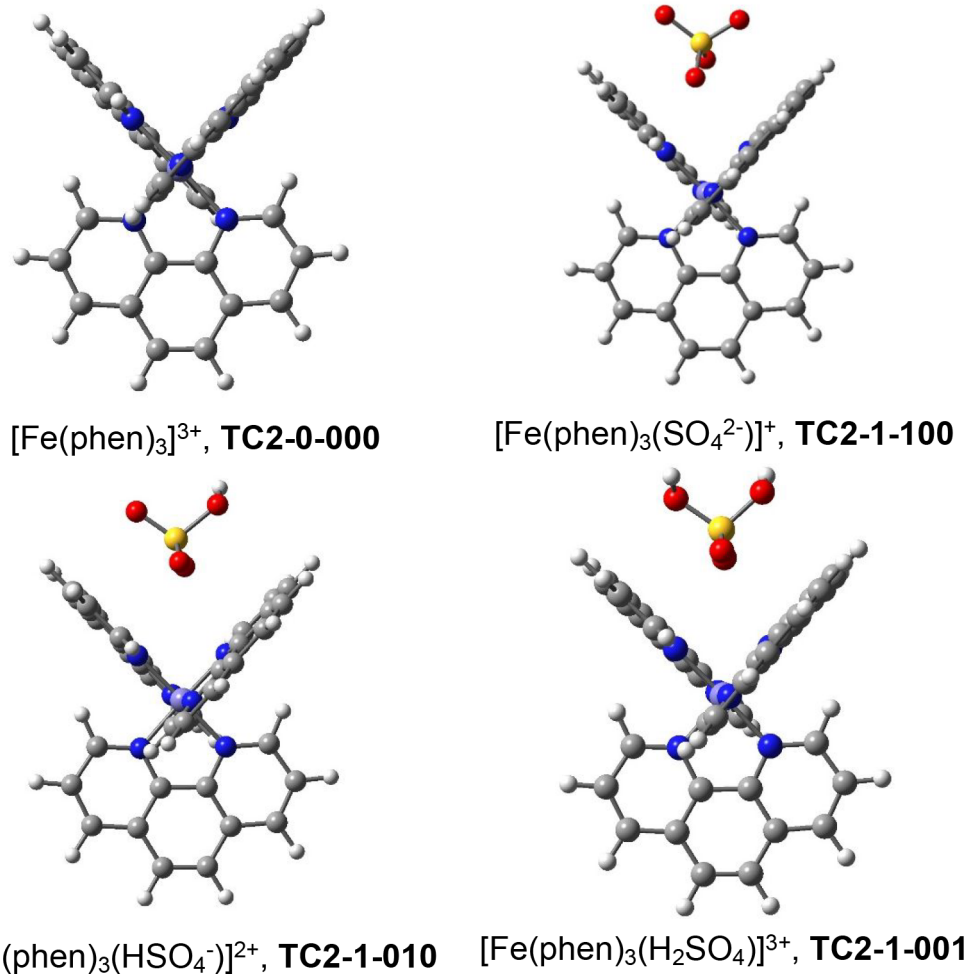

Figure 1. Molecular models computed at the SMD(APFD/6-311G*) level of ferriin and its aggregates with sulfate, bisulfate, and sulfuric acid.

SMD(APFD/6-311G*). In a few cases, we encountered convergence problems at the SMD level. In those cases, we report SMD(APFD/6-311G*)//APFD/6-311G* data; that is, we report SMD(APFD/6-311G*) total energies computed with the APFD/6-311G* structures and employ thermochemical data obtained at the APFD/6-311G* level. All computations were performed with *Gaussian16*[48] on the Lewis cluster of the University of Missouri.

We optimized all systems in their two lowest spin multiplicities. We will show that the spin density is localized at iron, that the spin state has negligible effect on structures, and that the low-spin systems are preferred at both oxidation states. Cartesian coordinates of all optimized structures obtained with both multiplicities are provided in Supporting Information, and the structures of the low-spin systems are discussed below. Total energies and thermochemical data of ferriin and ferroin systems, respectively, are collected in Tables S1 and S2 in the Supporting Information. Total energies and thermochemical data for sulfate, bisulfate, and sulfuric acid are shown in Table S3. Each table contains total energies in hartree, vibrational zero-point energies (VZPE) in kcal/mol, thermal energies (TE) in kcal/mol, molecular entropies (S) in kcal·mol^{-1}·K^{-1}, the lowest vibrational frequencies (ν_1) in wave numbers (cm^{-1}), and molecular dipole moments in debye.

The energies computed for ferriin and ferroin systems with the same aggregation were employed to compute ionization energies of ferroin. Three ionization energies were determined. We first computed the adiabatic ionization energy (IE) with the fully relaxed structures of the ferroin and ferriin systems (ΔG and ΔE of reaction 2). We also computed vertical ionization energies of the ferroin systems (VIE), as well as the vertical electron affinities of the ferriin systems (VEA). In Table S1, we included the energies of the ferriin system using a ground state structure of the corresponding ferroin system, and in Table S2 we included the energies of the ferroin system computed using ground state structures from the corresponding ferriin system.

3. RESULTS AND DISCUSSION

3.1. Nomenclature for Complex Constitution. We studied iron-phenanthroline complexes of +2 and +3 oxidation states. In each complex, the central iron atom was surrounded with three phenanthroline ligands and aggregated with counterions of varying number and protonation state and/or neutral species. Specifically, ferriin and ferroin were aggregated with sulfates, bisulfates, and sulfuric acids. The nomenclature system that we devised contains three groups of information, each separated by a dash. For example, **TC2-3-012** denotes an aggregate formed by the **trication (TC)** ferriin in its **doublet state (2)** aggregated with **three species**, of which there are **zero sulfate, one bisulfate, and two sulfuric acid ligands**. In the case where the iron has a +2 charge, the first letters would be DC, for dication. The trication systems were studied with doublet (TC2) and quartet (TC4) multiplicities, and the

https://doi.org/10.1021/acs.jpca.2c05879
J. Phys. Chem. A 2022, 126, 7261−7272

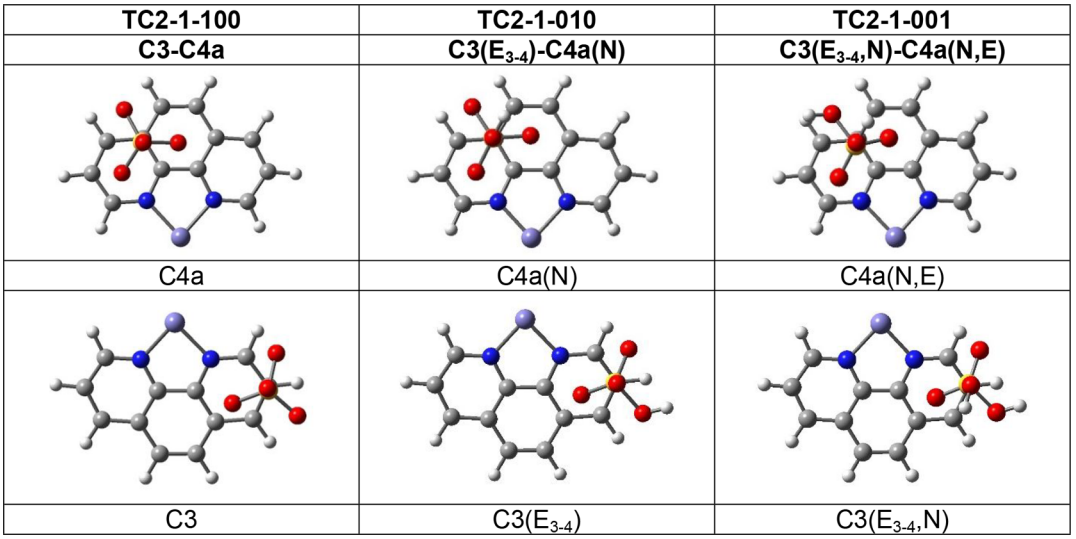

Figure 2. Regiochemisty of the OSL-ligand interaction. See text for a description of the coordination modes.

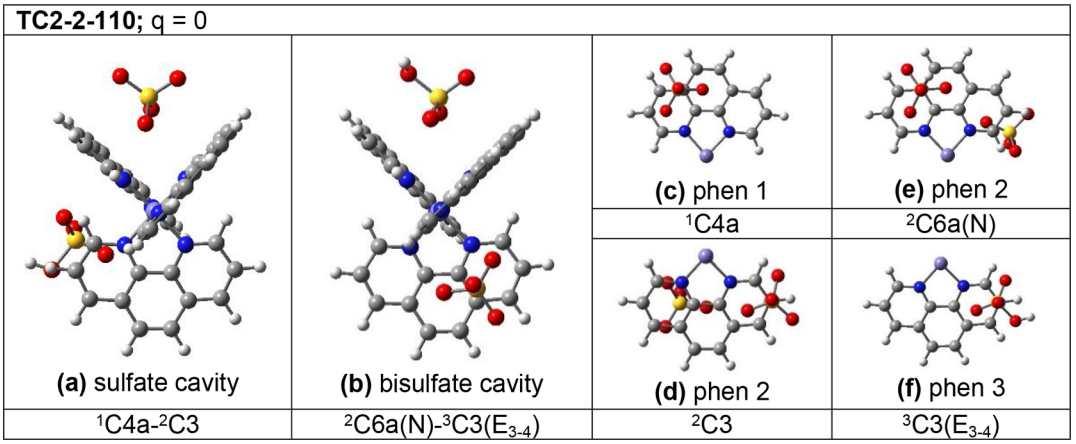

Figure 3. Molecular model of **TC2-2-110** computed at the SMD(APFD/6-311G*) level of ferriin doublet in its aggregate with the two OSLs sulfate and bisulfate. The cavity views emphasize the placement of one OSL between two phen ligands, and the four images on the right emphasize the placement of the two OSLs relative to one phen ligand. See text for structural descriptors.

dication systems were studied with singlet (DC1) and triplet (DC3) multiplicities.

3.2. Structures of Ferriin $[Fe(phen)_3]^{3+}$ and its Aggregates. *3.2.1. Ferriin Aggregates with One Ligand.* The structures of ferriin doublet and its aggregates with sulfate, bisulfate, and sulfuric acid are shown in Figure 1. The structure of ferriin doublet shows the expected coordination with 1,10-phenanthroline (phen). In Figure 1, the structure is projected in a way that emphasizes the cavity between two phenanthroline ligands.

As can be seen, the sulfate species is positioned between the phenanthrolines in such a way that three oxygen atoms interact with the face of each ligand. Moreover, the best plane of the three coordinating oxygen atoms is almost coplanar with the plane of the coordinated phenanthroline in both OSL−ligand interactions.

The projection in Figure 2 illustrates the regiochemistry of the OSL−ligand interaction. Two distinct coordination modes become apparent. With all ligands, there is one common coordination mode (Figure 2, top row) in which the sulfur is placed above the C4a atom, and one S−O bond is nearly perpendicular to, and pointing away from, the phen ligand. Of the three oxygens in the plane parallel to the phenanthroline, only two are positioned roughly above the centers of one pyridine ring and the benzene ring, respectively. The third oxygen is located above the bay area defined by (C4)H−C4a−(C5)H, and it is external to the phenanthroline's π cloud. These three oxygens are placed in a staggered conformation when viewed down the S−C(4a) axis. We will refer to this type of coordination as the C4a mode. The other coordination mode (Figure 2, bottom row) is similar, but the sulfur is centered above the C3 atom, and the oxygens again show the staggered conformation about the S−C3 axis (C3 mode).

There are several options for the placement of any OH group relative to the face of the coordinated phenanthroline. For the bisulfate ligand (Figure 2, top center), the C4a mode is realized with the unique OH group not coordinating to the face of the phen ligand; the C4a(N) mode, where the "N" descriptor indicates that the OH oxygen is noncoordinating relative to the phen ligand. For the sulfuric acid ligand (Figure 2, top right), the coordination mode is C4a(N,E), where the "E" descriptor indicates that the second OH group is located externally to the phenanthroline. In the C3 mode, only one oxygen is located above one pyridine ring, while the other two

https://doi.org/10.1021/acs.jpca.2c05879
J. Phys. Chem. A 2022, 126, 7261−7272

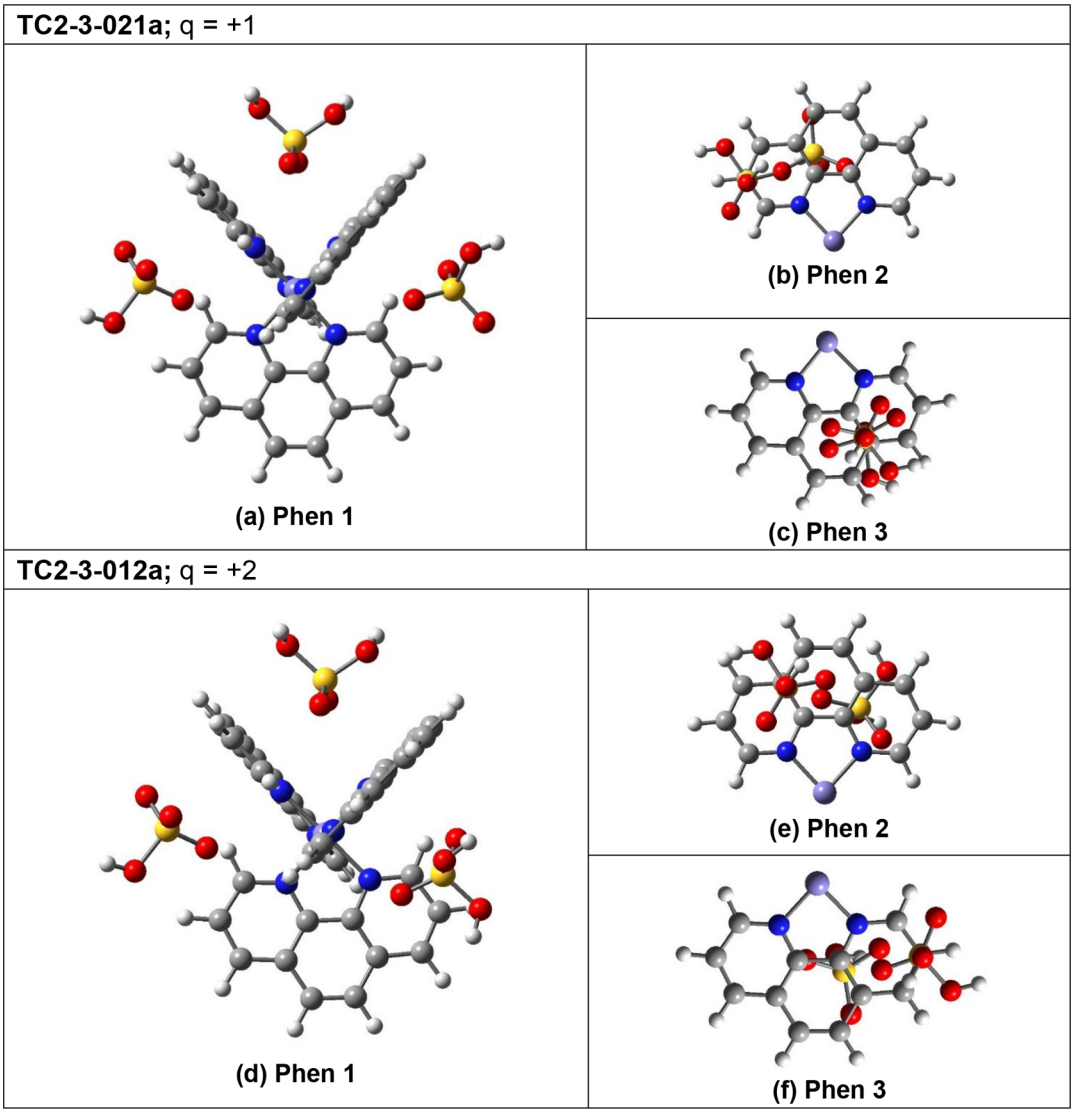

Figure 4. Molecular models of aggregates **TC2-3** computed at the SMD(APFD/6-311G*) level of ferriin doublet in its aggregates with three OSLs of bisulfate and sulfuric acid. **TC2-3-021a** (top), with two bisulfates and one sulfuric acid, and **TC2-3-012a** (bottom), with one bisulfate and two sulfuric acids.

oxygens are external. One of the oxygens is close to the C2−C3 bond in the E_{2-3} location, and the other is close to the C3−C4 bond in the E_{3-4} location. For the bisulfate ligand (Figure 2, bottom center), for example, the coordination mode is C3(E_{3-4}).

A complete description of the aggregation of one OSL ligand with an $[Fe(phen)_3]^{2+}$ complex requires the specification of both of its coordination modes. For the bisulfate complex **TC2-1-010**, for example, the complete description would be C3(E_{3-4})-C4a(N). For the sulfuric acid complex **TC2-1-001**, the complete description would be C3(E_{3-4},N)-C4a(N,E).

3.2.2. Ferriin Aggregates with Two Ligands. The structural description of aggregates with two or more OSL ligands requires numbering of the phenanthrolines and additional consideration of the coordination modes of two OSL ligands with one and the same phenanthroline. If possible, phenanthroline numbering starts with a phenanthroline coordinating to one OSL ligand only. The direction of the numbering will always be such that the next phenanthroline will be coordinated by two OSL ligands. We choose to give highest priority to the phenanthroline interacting with OSL ligands of highest combined negative charge. The assigned number of the phenanthroline will be added as a superscript before the mode descriptor. The sequence of mode descriptors will follow the phenanthroline numbering.

For phenanthrolines with double OSL coordination, one has to differentiate between the pyridine moieties. The numbering within a phenanthroline coordinated by just one OSL will always aim to minimize the location number. For phenanthrolines coordinated by two OSLs, a "C4a" contact may become a "C6a" mode if the two OSL ligands coordinate to different pyridines. Similarly, a "C3" contact may become a "C8" contact.

In Figure 3, we show various perspectives of **TC2-2-110**, and we will discuss this aggregate in detail to define the structural description. The scope of our study and the structural complexity of each aggregate prevents us from providing similar figures and discussion for the many molecules studied. Similar figures for the other **TC2-2** aggregates are provided as Supporting Information (Figure S1). Instead, in

https://doi.org/10.1021/acs.jpca.2c05879
J. Phys. Chem. A 2022, 126, 7261−7272

Table S4, a summary is provided that fully describes the topological features of all aggregates, with information about the coordination modes for sulfate, bisulfate, and sulfuric acid ligands in that sequence. Several rows are used to describe multiple occurrences of the same ligand.

In Figure 3, two perspectives are shown of aggregate **TC2-2-110** that highlight the positioning of the sulfate (a) and bisulfate (b) in their respective phenanthroline cavities. This aggregate features two phenanthrolines with single-OSL complexation and one phenanthroline with double-OSL complexation. Sulfate is the most anionic OSL, and determines the identity of phenanthroline 1. The coordination mode of the sulfate is ^{1}C4a−^{2}C3, shown in panels c and d. The bisulfate coordination is described by ^{2}C6a(N)−^{3}C3(E_{3-4}), shown in panels e and f. Note that sulfate and bisulfate engage different pyridines in phenanthroline 2. The first OSL engages phenanthroline 2 with a ^{2}C3 contact, and hence the "C4a(N)" contact of the bisulfate becomes a "C6a(N)" contact.

The same kind of analysis of the other three complexes of **TC2-2-020**, **TC2-2-011**, and **TC2-2-002** results in the coordination mode descriptors listed in Table S4. A first insight from this structural analysis is the suggestion that double coordination of one phenanthroline appears to prefer OSL engagements at the two ends of the phenanthroline.

3.2.3. Ferriin Aggregates with Three Ligands. We optimized six ferriin aggregates with three OSLs. Four of these structures feature new types of coordination, and two representatives of these structures are shown in Figure 4. In Supporting Information, we provide cavity views of all six **TC2-3** aggregates in Figure S2. In **TC2-3-030** and **TC2-3-003**, all OSLs are either bisulfates or sulfuric acids, respectively, and there is no issue of sequence isomerism. The aggregates with two identical ligands give rise to sequence isomers, because of the arrangement of the OSLs. In **TC2-3-021a**, the identical ligands both interact with **Phen 1**, but in **TC2-3-021b**, the unique ligand interacts with **Phen 1**. In **TC2-3-012a**, the unique ligand interacts with **Phen 1**, but in **TC2-3-012b**, the identical ligands both interact with **Phen 1**.

In the top half of Figure 4, molecular models are displayed of **TC2-3-021a**. A novel coordination mode is displayed by **Phen 1** (Figure 4a, bottom), in that neither of the OSLs engages in face coordination. The OSLs remain on different sides of the phenanthroline plane but their interaction is with the periphery of the **Phen 1** ligand. The bisulfate on the right side of **Phen 1** in Figure 4(a) is closest to the viewer, and engages in hydrogen bonding between one of its oxygens and the positively polarized hydrogen of the C(2)H group (2.273 Å). The other bisulfate is on the far side and engages in the same kind of hydrogen bonding with the C(9)H group (2.231 Å). This mode of coordination is referred to as the "H" mode, and the location is indicated with a subscript. Note the difference in the protonation sites of the bisulfates engaged in the H_{C2H} and H_{C9H} contacts.

In earlier examples, double-OSL coordination of a phenanthroline ligand involved different pyridine moieties of the phen ligand (see Figure 3). It is one important consequence of the double-H coordination of **Phen 1** that phen ligands **2** and **3** in **TC2-3-021a** are face-coordinated each with two OSLs coordinating to the *same* region of the phenanthroline. **Phen 2** shows C8 coordination with the sulfuric acid and C4a coordination with the bisulfate (Figure 4b), and **Phen 3** shows bifacial C4a coordination (Figure 4c).

TC2-3-012a shows one H contact of the type seen in **TC2-3-021a**, while the other OSL features a more common C3 coordination. The bisulfate on the left side of **Phen 1** (Figure 4d) engages in hydrogen bonding with the C(9)H group (2.409 Å).

Hydrogens in OSLs that show the H coordination mode are referred to using their relation to the coordination mode of the other phenanthroline ligand. For example, **TC2-3-021a** shows H_{C9H} coordination with **Phen 1**, and C6a coordination with **Phen 2**. Thus, the H_{C9H} hydrogen is considered "N" because the coordination mode with **Phen 2** is C6a(N).

3.3. Structures of Ferroin $[Fe(phen)_3]^{2+}$ and its Aggregates. The ferroin singlet structures are topologically and structurally analogous to their respective ferriin aggregates. The structural similarity is so striking that no detailed structural description of the ferroin structures is warranted. Hence, in Table S5, we provide a summary that fully describes the topological features of all ferroin aggregates in complete analogy to Table S4 describing ferriin structures.

3.4. Spin State Preferences. *3.4.1. Ferroin Singlet/Triplet and Ferriin Doublet/Quartet Gaps.* Fe^{2+} and Fe^{3+} complexes exist in a wide range of spin states, and the most commonly observed spin states are the low-spin configurations.[49] XPS studies of Fe^{2+} complexes found that $[Fe(phen)_3]^{2+}$ exists as a low-spin singlet in the ground state and that substituents on phenanthroline can distort the coordination sphere and affect the spin state.[50] Specifically, Burger et al. showed that the triplet state can exist as the ground state in certain iron complexes with substituted phenanthrolines.[50] This result was also found in studies of magnetic moments of mixed bis-phenanthroline $Fe(phen)_2X_2$ complexes.[51] More recent work has demonstrated examples of Fe^{3+} complexes with a quartet ground state.[52] A common theme in these findings is that triplet and quartet spin states in Fe^{2+} and Fe^{3+}, respectively, play important roles in certain biological systems.[53] To ensure the identity of the ground states of the ferriin and ferroin complexes, we compared the doublet and quartet spin states in ferriin systems and the singlet and triplet spin states in ferroin systems. The results in Table 1 clearly show that the low-spin multiplicity is preferred by around 10 kcal/mol in ferriin systems and by 6−8 kcal/mol in ferroin systems. In the following, all discussions are based on the singlet in ferroin systems and the doublet in ferriin systems.

Table 1. Spin-State Preferences of Ferriin and Ferroin Complexes[a]

ferriin trication doublet−quartet gap		ferroin dication singlet−triplet gap	
structure	ΔG	structure	ΔG
TC-0-000	12.39	**DC-0-000**	34.94
TC-1-100	11.63	**DC-1-100**	6.66
TC-1-010	10.88	**DC-2-110**	8.01
TC-1-001	10.65	**DC-1-010**	6.06
TC-2-110	10.96	**DC-1-001**	9.49
TC-2-020	10.62	**DC-2-020**	7.20
TC-2-011	11.06	**DC-2-011**	8.77
TC-2-002	11.18	**DC-2-002**	21.90
TC-3-030	8.87	**DC-3-030**	5.17
TC-3-021	10.02	**DC-3-021**	6.31
TC-3-012	9.95	**DC-3-012**	5.26
TC-3-003	10.85	**DC-3-003**	8.97

[a]Relative free energies ΔG in kcal/mol.

https://doi.org/10.1021/acs.jpca.2c05879
J. Phys. Chem. A 2022, 126, 7261−7272

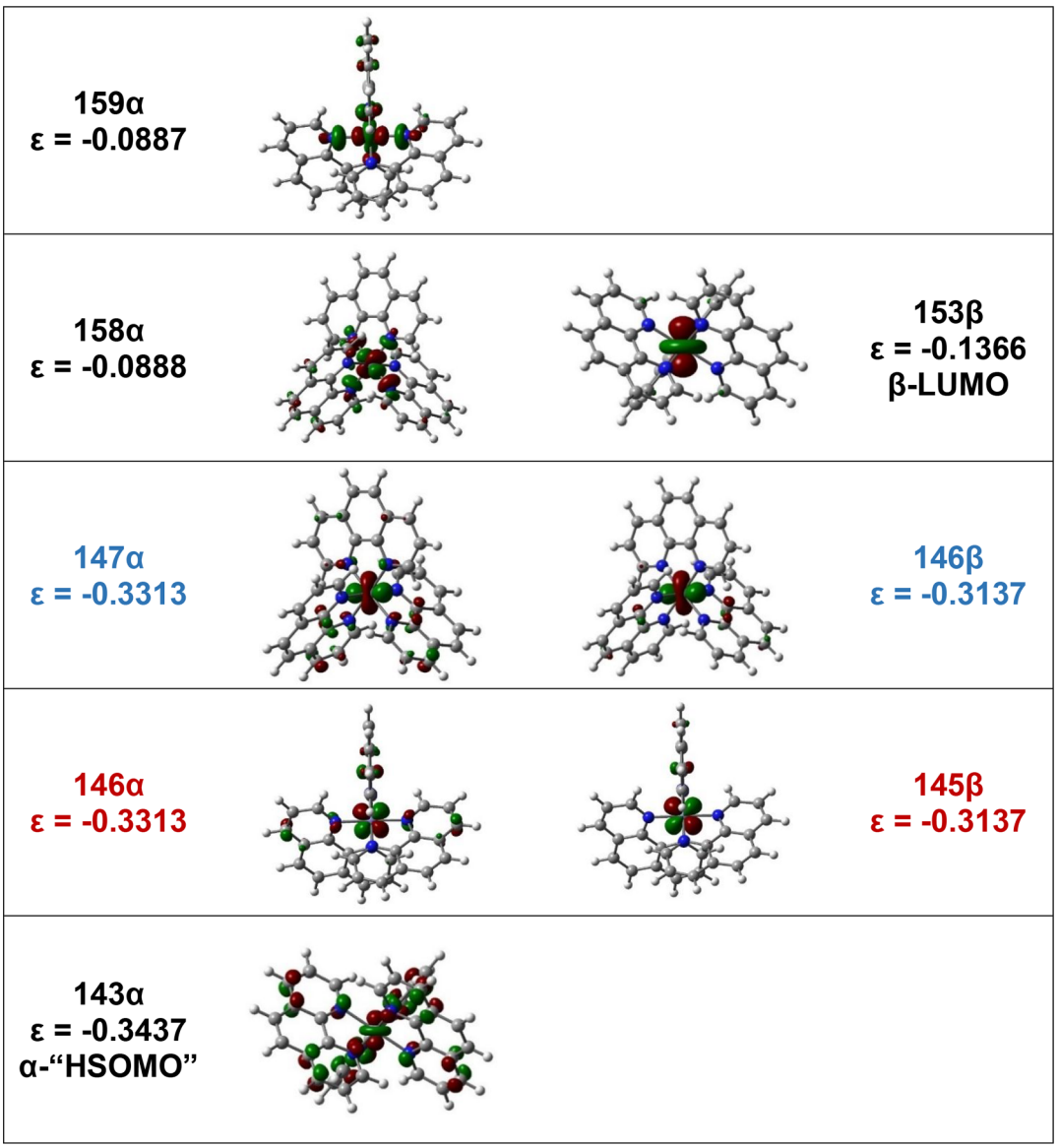

Figure 5. Isosurface plots (isovalue = 0.05 e/au^3) are shown of the iron d-orbitals of the α-spin electron (left) and β-spin electrons (right) of the trication doublet **TC2-0-000**. Molecular orbital eigenvalues ε_i (in eV) increase from the bottom up.

3.4.2. Spin Density Distributions. The spin density distribution is easily rationalized by molecular orbital (MO) theory.[54] We analyzed the α- and β-MOs of the unrestricted wave function of the doublet trication and identified two near-perfectly paired and degenerate d-MOs. Figure 5 shows that MOs 147α and 146β have almost the same shape, and the same is true for MOs 146α and 145β. The unpaired electron at iron occupies MO 143α, and the corresponding β-MO is the LUMO of the β-set, MO 153β. The MO 143α can be described as the α-"HSOMO" (highest singly occupied molecular orbital) because there is no occupied β-orbital of that shape.

Note that the unpaired d-electron is *more* stable than both of the near-perfectly paired d-orbitals. The MO 143α is the HSOMO (highest singly occupied/unpaired MO) with an eigenvalue of $\varepsilon = -0.3437$ eV. There are *six* α-MOs (148α–153α) above the highest occupied d-orbital in the α-set (147α), and the analogous occurs in the β-set; that is, six occupied π-orbitals of the phenanthroline ligands are above the iron d-electrons. While textbooks routinely propagate the notion that the radical electron must, as a rule, occupy the HOMO, clearly this idea is misguided in the present case, as in many others.[55−57]

Contour plots of the total spin density distribution ρ_s of the doublet trication systems are shown in Figure 6. The spin density is localized at iron and is well described as a d_{z^2}-shaped region, as expected based on the shape of the HSOMO. Figure 6 also includes the total spin densities of the quartet and sextet states of ferriin. The geometries of the spin states were optimized and confirmed that the spin state has essentially no effect on structure. The MO analysis illustrates that the electron configuration of the quartet arises by moving one electron from MO 146β into MO 158α. Furthermore, the electron configuration of the sextet arises from the quartet by also elevating an electron from MO 145β into MO 159α. In the sextet state, each iron d-orbital is singly occupied, and the spin density at iron is almost spherically symmetric. The shape of the total α-spin density of the quartet state reflects that a d_{xy} shaped region is occupied by an α- and a β-electron (MO 146α and MO 145β).

https://doi.org/10.1021/acs.jpca.2c05879
J. Phys. Chem. A 2022, 126, 7261−7272

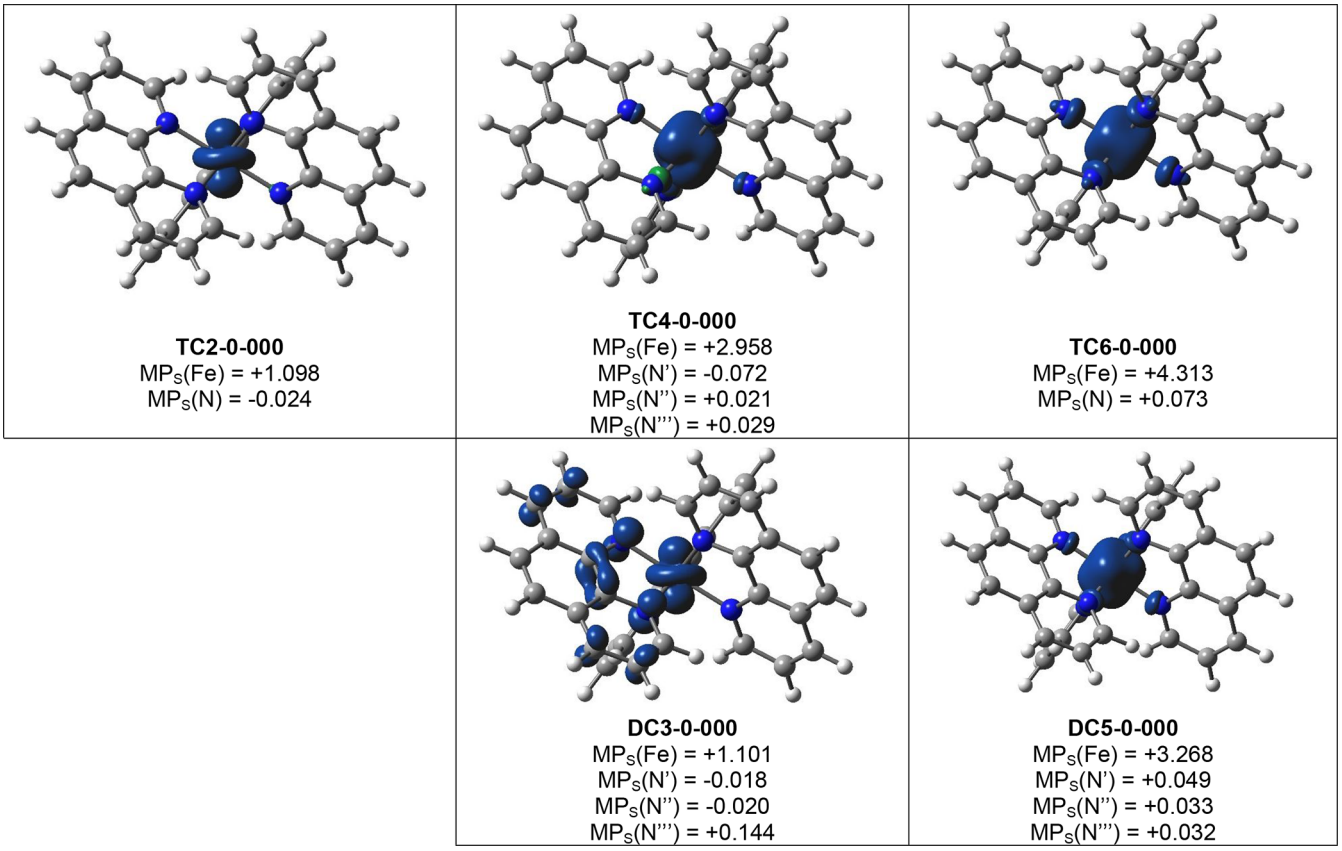

Figure 6. Spin density distribution of ferriin doublet, quartet, and sextet (top row), and ferroin triplet and quintet (bottom row). Spin density contoured at ρ_s = 0.008 α-e/a.u.[3]

The most pertinent results of Mulliken population analyses of the wave functions of the Fe^{3+} species are included in the top row of Figure 6. The total Mulliken spin population of Fe^{3+} ($MP_S(Fe)$) in the doublet **TC2-0-000** is slightly more than unity, and the N atoms feature a small excess of β-spin density because of spin-polarization. In contrast, in the sextet system, the spin population at iron is less than five because of spin-density delocalization onto the N atoms. The quartet system is in between with two N atoms featuring excess β-spin (compare the green regions in Figure 6), while the other nitrogens carry small amounts of α-spin. The Fe^{2+} species show the same trend (Figure 6, bottom row).

3.5. Ligand Binding Energies. The computed OSL binding energies are summarized in Table 2. For example, the binding of the first bisulfate to singlet ferroin **DC1-0-000** to form **DC1-1-010** is exergonic by 11.8 kcal/mol and its binding to doublet ferriin **TC2-0-000** to form **TC2-1-010** is exergonic by 16.7 kcal/mol.

The binding energies do not follow simple intuition in that the charge of the OSL affects the binding energy only moderately. There appears to be a trend to suggest that the binding of the *second* OSL is stronger than the binding of the first OSL, and that the third OSL is bound the least. The main message of the data in Table 2 is that the average OSL binding free energies are estimated to be in the ranges of 12.4 ± 2.5 kcal/mol for ferroin and 14.3 ± 2.5 kcal/mol for ferriin. The binding energies are of an order of magnitude that clearly implicates the involvement of outer sphere ligation in the iron-catalyzed Belousov–Zhabotinsky reaction and shows that OSL binding processes are reversible equilibria.

Table 2. Outer Sphere Ligand Binding Energies of Ferroin and Ferriin Complexes with Sulfate, Bisulfate, and Sulfuric Acid[a]

			ferroin	ferriin
OSL	starting structure	ending structure	OSLBE[b]	OSLBE
SO_4^{2-}	**0-000**	**1-100**	12.62	18.57
HSO_4^-	**0-000**	**1-010**	11.80	16.68
H_2SO_4	**0-000**	**1-001**	13.93	13.77
SO_4^{2-}	**1-010**	**2-110**	15.38	17.10
HSO_4^-	**1-100**	**2-110**	14.57	15.22
HSO_4^-	**1-010**	**2-020**	14.98	15.65
HSO_4^-	**1-001**	**2-011**	14.15	17.22
H_2SO_4	**1-010**	**2-011**	16.28	14.31
H_2SO_4	**1-001**	**2-002**	13.93	15.03
HSO_4^-	**2-020**	**3-030**	9.91	10.42
HSO_4^-	**2-011**	**3-021**	9.32	11.17
HSO_4^-	**2-002**	**3-012**	8.92	14.57
H_2SO_4	**2-020**	**3-021**	10.62	9.83
H_2SO_4	**2-011**	**3-012**	8.70	12.38
H_2SO_4	**2-002**	**3-003**	10.62	12.05

[a]Binding free energies ΔG in kcal/mol. [b]OSLBE abbreviates "Outer Sphere Ligand Binding Energies."

3.6. Ferroin–Ferriin Redox Energies. Computed energies associated with iron redox processes are compiled in Table 3, and they include adiabatic ionization energies (AIE), vertical ionization energies (VIE), and vertical electron affinities (VEA). For the AIE, the computed ΔG and ΔE values are very similar, and we only discuss the ionization

https://doi.org/10.1021/acs.jpca.2c05879
J. Phys. Chem. A 2022, 126, 7261–7272

Table 3. Adiabatic Ionization Energies (AIE), Vertical Ionization Energy (VIE), and Vertical Electron Affinity (VEA)[a]

	AIE			
structure	ΔG	ΔE	VIE	VEA
0-000	112.8	112.7	112.7	111.7
1-100	106.9	106.8	111.6	107.9
1-010	108.3	107.9	112.6	109.2
1-001	113.3	112.9	115.8	111.1
2-110	106.9	106.1	109.8	106.0
2-020	108.4	107.2	107.2	106.9
2-011	111.3	109.8	113.5	108.6
2-002	113.0	111.8	112.4	110.4
3-030	106.5	106.7	108.9	106.0
3-021a	108.4	108.0	110.2	107.5
3-021b	108.8	108.3	112.5	106.8
3-012a	107.7	106.1	111.6	108.7
3-012b	111.0	109.7	110.9	108.4
3-003	110.9	110.4	112.5	110.1

[a]All values in kcal/mol.

energies. As expected, the ionization energy of the dication complex is lowered by the presence of an anionic ligand and more so with increasing negative charge on that ligand (ΔE in Table 3). The ionization energies AIE are 106.8 kcal/mol for the sulfate aggregate **1-100**, 107.9 kcal/mol for the bisulfate aggregate **1-010**, 112.9 kcal/mol for the sulfuric acid aggregate **1-001**, and virtually identical with the unaggregated parent complex **0-000**. The effects of several OSLs very clearly are *not* additive. For example, the ionization of **2-110** is 106.1 kcal/mol and very close to that of **1-100**; the bisulfate as a second OSL is much less effective at lowering the AIE than it is as a first OSL. With the presence of three OSLs, the destabilization associated with the repulsion between the OSLs is felt more in the Fe^{2+} systems than in the Fe^{3+} systems and limits the OSL related reduction of the ionization energy.

The vertical ionization energies (VIE) have to be larger compared to the adiabatic ionization energies (AIE), and Table 3 quantifies these increases. In aggregates with just one ligand, the increase is the largest, and the effect is more moderate in complexes with more OSLs. It is also noticeable that the difference between AIE and VIE grows in the order of sulfate > bisulfate > sulfuric acid.

In the context of oscillating chemical reactions, the most interesting redox parameter is VEA, the vertical electron affinity. In the key step of the iron-catalyzed Belousov–Zhabotinsky reaction (reaction R9), the high-oxidation state iron, ferriin, must be reduced by a brominated organic acid "fuel." We have found in our previous experimental work that this ferriin reduction is proton-catalyzed.[21] This finding suggested that the VEA values of OSL complexes of ferriin should *increase* upon OSL protonation. Indeed, this expectation is borne out in the computed data. The sulfate complex of ferriin **1-100** exhibits a VEA of 107.9 kcal/mol, and the VEA increases to 109.2 and 111.1 kcal/mol upon single and double protonation, respectively. The same trend is confirmed for ferriin complexes with two and three OSLs. Considering that reaction R9 is thought to be marginally exothermic with $\Delta G \approx -1.4$ kcal/mol, the Hammond postulate[58,59] suggests that any substantial increase in the reaction exothermicity should manifest itself substantially in the activation barrier of the redox reaction.

3.7. Proton Affinities of Anionic OSLs in Ferriin Aggregates. We are interested in the proton affinities of the OSLs in the various ferriin aggregates. The direct calculation of the proton affinity of substrate A via reaction 3 requires knowledge of $\Delta G(H^+)$, which is notoriously difficult to compute accurately. A better result can be achieved by determination of ΔG_{3a} of reaction 3a. But even then, the solvated proton is not well represented. Instead, we evaluate reaction 3 based on the reaction energy of reaction 3a and the experimental value for the proton affinity of water; $\Delta G_3 = \Delta G_{3a} + \Delta G_4 = \Delta G_{3a} - PA(H_2O)$.

$$A + H^+ \rightarrow AH^+ \quad (3)$$

$$A + H_3O^+ \rightarrow AH^+ + H_2O \quad (3a)$$

$$H_2O + H^+ \rightarrow H_3O^+ \quad (4)$$

$$\Delta G_3 = \Delta G(AH^+) - \Delta G(A) - \Delta G(H^+) \quad (I)$$

$$\Delta G_{3a} = \Delta G(AH^+) + \Delta G(H_2O) - \Delta G(A) - \Delta G(H_3O^+) \quad (Ia)$$

$$\Delta G_4 = \Delta G(H_3O^+) - \Delta G(H_2O) - \Delta G(H^+) \quad (II)$$

$$PA(A) = PA(H_2O) - \Delta G_{3a} \quad (III)$$

We use the proton affinity of water $PA(H_2O) = 165.2 \pm 0.7$ kcal/mol recommended by Hunter *et al.*,[60] which was adopted by the National Institute of Standards and Safety (NIST). There has been an ongoing discussion about the proton affinity of water, and these are briefly summarized in Table S6 in the Supporting Information. We evaluated the reaction energies ΔG_{3a} for a variety of ferriin aggregates A via eq Ia to determine their proton affinities PA(A) via eq III, and the results are summarized in Table 4. For water, sulfate, and bisulfate, literature values of ΔG_{3a} are reported.[61,62]

Table 4. Relative Gibbs Free Energy of Protonation, Proton Affinity, and Relative Proton Affinities of Structures of Ferriin Doublets[a]

ferriin aggregate A	protonated ferriin aggr. AH^+	prot. rxn ΔG_{3a}	proton affinity PA(A)
H_2O	H_3O^+	−0.96[b]	165.2[c]
SO_4^{2-}	HSO_4^-	−2.62[d]	167.82
HSO_4^-	H_2SO_4	4.09[d]	161.18
TC2-1-100	**TC2-1-010**	−23.99	189.19
TC2-1-010	**TC2-1-001**	2.58	162.62
TC2-2-110	**TC2-2-020**	−23.89	189.09
TC2-2-020	**TC2-2-011**	1.24	163.96
TC2-2-011	**TC2-2-002**	2.49	162.71
TC2-3-030	**TC2-3-021**	0.88	164.32
TC2-3-021	**TC2-3-012**	−0.69	165.89
TC2-3-012	**TC2-3-003**	2.69	162.51

[a]All values in kcal/mol. [b]See ref 61. [c]See ref 60. [d]See ref 62.

Reaction 2 provides a specific example for the protonation of complex **TC2-1-010** leading to **TC2-1-001**. The proton affinity of **TC2-1-010** equals the negative reaction energy ΔG_2 of reaction 2, PA(**TC2-1-010**).

The proton affinity of the sulfate ligand in any ferriin aggregate is over 20 kcal/mol higher than the proton affinity of water. These numbers are so large that it is safe to conclude that ligation by sulfate ions has an exceedingly low probability.

https://doi.org/10.1021/acs.jpca.2c05879
J. Phys. Chem. A 2022, 126, 7261−7272

Therefore, our focus turns on double-protonation chains (DPC) that start with OSL adducts without sulfate and enough bisulfate OSLs to make double-protonation an option. There are three such double-protonation chains. For the aggregates **TC2-2** with two OSLs, there is only one path for double-protonation (DPC1), and it leads from **TC2-2-020** to **TC2-2-011** and finally to **TC2-2-002** (VEA = 110.4 kcal/mol). Both of these protonation reactions are slightly endothermic with ΔG_{3a} values of 1.24 and 2.49 kcal/mol, respectively, and the energy of the overall double-protonation is +3.73 kcal/mol. For the aggregates **TC2-3** with three OSLs, there are two double-protonation chains. The DPC2 path is **TC2-3-030** → **TC2-3-021** → **TC2-3-012** (VEA = 108.4 kcal/mol), and the DPC3 path is **TC2-3-021** → **TC2-3-012** → **TC2-3-003** (VEA = 110.1 kcal/mol). The relevant protonation energies are included in Table 4. The overall protonation energies for the two pathways are +0.19 and +2.00 kcal/mol, respectively.

The most relevant double-protonation paths are decided by the combined effects of the required energy for double-protonation and the VEA of the double-protonated aggregate. The ideal DPC would have a low double-protonation energy and a high VEA of the double-protonated adduct. While DPC1 offers high VEA of **TC2-2-002** of 110.4 kcal/mol, this path has the disadvantage of requiring the highest double-protonation energy. For paths DPC2 and DPC3 the two parameters could indicate preferences for one or the other: the double-protonation energy is about 1.8 kcal/mol lower for DPC2 compared to DPC3, but the VEA associated with DPC3 offers almost the same energy payoff of about 1.7 kcal/mol. Perhaps the only conclusion we can make with some certainty is that paths DPC2 and DPC3 are thermodynamically plausible paths for double-protonation and are favored over path DPC1.

4. CONCLUSION

Traditionally, studies of Belousov–Zhabotinsky oscillating reactions have focused on the role of the metal catalyst and/or the organic "fuel." Our recent kinetic studies of the pH dependence of the iron-catalyzed Belousov–Zhabotinsky reaction revealed that the reduction of ferriin is subject to second-order proton catalysis. For the first time, we have considered the role of outer sphere ligation in the mechanism. We present compelling evidence that outer sphere ligation plays an important role in the iron-catalyzed Belousov–Zhabotinsky reaction using density functional studies of ferriin and ferroin complexes with the consideration of bulk aqueous solvation at the SMD(APFD/6-311G*) level. We explored potential energy surfaces of ferriin and ferroin aggregates with *m* sulfate ligands, *n* bisulfate ligands, and *o* sulfuric acid ligands (detailed in reaction 2), and all of those structures were discussed thoroughly.

The structural discussion of OSL aggregates identifies types of noncovalent interactions between phenanthroline ligands and OSLs, and a nomenclature had to be developed to precisely describe the nature of the aggregation. The coordination modes of ferriin and ferroin aggregates consider all possibilities of OSL identity, placement relative to the phenanthroline ligands, and orientation. We investigated structures with the two lowest spin states, and as expected, the low-spin state is preferable in all systems. Since ferriin and ferroin aggregates of this type have never investigated in detail, we further characterized the aggregates' spin densities and relevant molecular orbitals. The most surprising result is that the highest singly occupied molecular orbital is more stable than both pairs of d-electrons.

We computed OSL binding energies and established that the binding energies are on the order of about 15 kcal/mol. OSL aggregation with the parent complex happens rapidly and reversibly in solution. Redox energies for ferriin and ferroin aggregates show that the vertical electron affinity of ferriin aggregates increases with number of OSLs and with OSL protonation. With a larger electron affinity, the reduction of ferriin happens more readily in the system. This result strongly suggests that double protonation of OSLs is responsible for the second-order proton catalysis of the ferriin reduction. Furthermore, proton affinities show that there are thermodynamically plausible paths to double-protonation.

Belousov–Zhabotinsky reactions are notorious for their complexity and resistance to quick explanations. Here we propose that outer sphere ligation plays a critical role in the mechanism of the iron-catalyzed Belousov–Zhabotinsky reaction and provides a substrate for second-order proton catalysis of the reduction of ferriin. Further experimental study of metal complexes aggregated with OSLs will reveal a new level of detail in the mechanism of Belousov–Zhabotinsky reactions. Many Belousov–Zhabotinsky reactions with metal catalysts have proved to be sensitive to pH, and complexation of OSLs with different metal centers may result in different mechanisms for reactions previously considered analogous. We have offered a glimpse into the possibilities for OSL aggregation, and hope that this new paradigm will provide novel avenues for research into Belousov–Zhabotinsky oscillating reactions.

■ ASSOCIATED CONTENT

Supporting Information

The Supporting Information is available free of charge at https://pubs.acs.org/doi/10.1021/acs.jpca.2c05879.

Tables of total energies and thermochemical data of ferriin $[Fe(phen)_3]^{3+}$ and ferroin $[Fe(phen)_3]^{2+}$ and their aggregates, and of coordination modes descriptors of trication doublets and dication singlets, figures showing molecular models of **TC2-2-020**, **TC2-2-011**, and **TC2-2-002** and cavity views of **TC2-3** aggregates, and a table summarizing literature about the proton affinity of water (PDF)

Cartesian coordinates of all stationary structures (PDF)

■ AUTHOR INFORMATION

Corresponding Author

Rainer Glaser − *Department of Chemistry, Missouri University of Science and Technology, Rolla, Missouri 65401, United States*; orcid.org/0000-0003-3673-3858; Email: glaserr@umsystem.edu

Author

Sara C. McCauley − *Department of Chemistry, Missouri University of Science and Technology, Rolla, Missouri 65401, United States*

Complete contact information is available at: https://pubs.acs.org/10.1021/acs.jpca.2c05879

Notes

The authors declare no competing financial interest.

https://doi.org/10.1021/acs.jpca.2c05879
J. Phys. Chem. A 2022, 126, 7261−7272

■ ACKNOWLEDGMENTS

This work was supported in part by funding from the National Science Foundation (1665487) and the Missouri University of Science and Technology. S.C.M. gratefully acknowledges support by the First Year Research Experience (FYRE) Program of the College of Arts, Sciences, and Business, by the Undergraduate Summer Research Scholarship (UGSRS) Program of the Department of Chemistry supported by the Peter H. Pietsch Memorial Scholarship and by the Carey & Christine Bottom Endowed Scholarship in Undergraduate Chemistry Research, and by the Opportunities for Undergraduate Research Experiences (OURE) Program of Missouri S&T. The computation for this work was performed on the high-performance computing infrastructure provided by Research Computing Support Services at the University of Missouri.

■ REFERENCES

(1) Kiprijanov, K. S. Chaos and beauty in a beaker: The early history of the Belousov-Zhabotinsky reaction. *Ann. Phys.* **2016**, *528*, 233−237.
(2) Koros, E.; Burger, M.; Friedrich, V.; Ladanyi, L.; et al. Chemistry of Belousov-Type Oscillating Reactions. *Faraday Symp. Chem. Soc.* **1974**, *9*, 28−37.
(3) Zhabotinsky, A. M.; Zaikin, A. N. Concentration Wave Propagations in Two-Dimensional Liquid-Phase Self-Oscillating System. *Nature* **1970**, *225*, 535−537.
(4) *An Introduction to Nonlinear Chemical Dynamics: Oscillations, Waves, Patterns, and Chaos*; Epstein, I. R., Pojman, J. A., Eds.; Oxford University Press: New York, 1998.
(5) Gray, P.; Scott, S. K.*Chemical Oscillations and Instabilities: Non-Linear Chemical Kinetics*; Oxford University Press: New York, 1994.
(6) Strogatz, S. H.*Nonlinear Dynamics and Chaos: With Applications to Physics, Biology, Chemistry, and Engineering (Studies in Nonlinearity)*; Westview Press: Boulder, CO, 2001.
(7) Gentili, P. L. Small steps towards the development of chemical artificial intelligent systems. *RSC Adv.* **2013**, *3*, 25523−25549.
(8) Gorecki, J.; Gizynski, K.; Guzowski, J.; Gorecka, J. N.; Garstecki, P.; Gruenert, G.; Dittrich, P. Chemical computing with reaction-diffusion processes. *Philos. Trans. R. Soc. A* **2015**, *373*, 20140219.
(9) Zhou, H.; Zheng, Z.; Wang, Q.; Xu, Q.; Li, J.; Ding, X. A modular approach to self-oscillating polymer systems driven by the Belousov-Zhabotinsky reaction. *RSC Adv.* **2015**, *5*, 13555.
(10) Yoshida, R. Self-oscillating polymer gels as biomimetic and smart softmaterials. *Adv. Mater. Lett.* **2018**, *9*, 836−842.
(11) Shakhashiri, B. Z.*Chemical Demonstrations*; The University of Wisconsin Press: Madison, WI, 1985; Vol. 2, p 257.
(12) Field, R. J.; Koros, E.; Noyes, R. M. Oscillations in Chemical Systems. II. Thorough Analysis of Temporal Oscillation in the Bromate-Cerium-Malonic Acid System. *J. Am. Chem. Soc.* **1972**, *94*, 8649−8664.
(13) Glaser, R. E.; Jost, M. Disproportionation of Bromous Acid HOBrO by Direct O-Transfer and via Anhydrides $O(BrO)_2$ and $BrO-BrO_2$. An Ab Initio Study of the Mechanism of a Key Step of the Belousov-Zhabotinsky Oscillating Reaction. *J. Phys. Chem. A* **2012**, *116*, 8352−8365.
(14) Glaser, R. E.; Downing, M.; Zars, E.; Schell, J.; Chicone, C.Video-Based Kinetic Analysis of Period Variations and Oscillation Patterns in the Ce/Fe-Catalyzed Four-Color Belousov-Zhabotinsky Oscillating Reaction. Chapter 15 in *It's Just Math: Research on Students' Understanding of Chemistry and Mathematics*. Towns, M. H., Bain, K., Rodriguez, J. G., Eds.; ACS Books: 2019; pp 251−270.
(15) Schell, J.; McCauley, S.; Glaser, R. E. Video colorimetry of single-chromophore systems based on vector analysis in the 3D color space: Unexpected hysteresis loops in oscillating chemical reactions. *Talanta* **2020**, *220*, 121303−121314.
(16) Glaser, R. E.; Delarosa, M. A.; Salau, A. O.; Chicone, C. Dynamical Approach to Multi-Equilibria Problems for Mixtures of Acids and Their Conjugated Bases. *J. Chem. Educ.* **2014**, *91*, 1009−1016.
(17) Zars, E.; Schell, J.; Delarosa, M.; Chicone, C.; Glaser, R. E. Dynamical Approach to Multi-Equilibria Problems Considering Debye-Hückel Theory of Electrolyte Solutions. Concentration Quotients as a Function of Ionic Strength. *J. Solution Chem.* **2017**, *46*, 643.
(18) Schell, J.; Zars, E.; Chicone, C.; Glaser, R. E. Simultaneous Determination of All Species Concentrations in Multi-Equilibria for Aqueous Solutions of Dihydrogen Phosphate Considering Debye-Hückel Theory. *J. Chem. Eng. Data* **2018**, *63*, 2151−2161.
(19) Foersterling, H. D.; Varga, M. Bromous acid/cerium(4+): reaction and HBrO2 disproportionation measured in sulfuric acid solution at different acidities. *J. Phys. Chem.* **1993**, *97*, 7932−7938.
(20) Ágreda B, J. A.; Field, R. J. Activation Energy for the Disproportionation of HBrO2 and Estimated Heats of Formation of HBrO2 and BrO2. *J. Phys. Chem. A* **2006**, *110*, 7867−7873.
(21) Zars, E.; Glaser, R. E.; Downing, M.; Chicone, C. Measurements and Simulations of the Acidity Dependence of the Kinetics of the Iron-Catalyzed Belousov-Zhabotinsky Reaction. Proton-Catalysis in the Electron Transfer Reaction Involving the $[Fe(phen)_3]^{3+}$ Species. *J. Phys. Chem. A* **2018**, *122*, 6183−6195.
(22) Adhikamsetty, R. K.; Gollapalli, N. R.; Jonnalagadda, S. B. Complexation kinetics of Fe^{2+} with 1,10-phenanthroline forming ferroin in acidic solutions. *Int. J. Chem. Kinet.* **2008**, *40*, 515−523.
(23) Potocnak, I.; Pohlova, M.; Wagner, C.; Jager, L. Tris(1,10-phenanthroline)copper(II) tricyanomethanide. *Acta Crystallogr. Sect. E* **2002**, *58*, m595−m596.
(24) Biswas, B.; Al-Hunaiti, A.; Raisanen, M. T.; Ansaloni, S.; Leskela, M.; Repo, T.; Chen, Y.; Tsai, H.; Naik, A. D.; Railliet, A. P.; et al. Efficient and selective oxidation of primary and secondary alcohols using an iron(III)/phenanthroline complex: Structural studies and catalytic activity. *Eur. J. Inorg. Chem.* **2012**, *2012*, 4479−4485.
(25) Qiu, X.; Yang, M.; Chen, W.; Su, Y.; Ouyang, Z.; Yan, H.; Gao, F.; Dong, W. Crystal Structures, UV Spectra of Solid Iodide Anionic Water Clusters $I^-(H_2O)_{1-4}$, and Electrochemical Reaction of $I^-(H_2O)_{1-4} \rightarrow I\cdot + e^-(H_2O)_{1-4}$. *J. Phys. Chem. A* **2013**, *117*, 4051−4056.
(26) Fu, Z.; Mi, C.; Sun, Y.; Yang, Z.; Xu, Q.; Fu, W. An Unexpected Iron (II)-Based Homogeneous Catalytic System for Highly Efficient CO_2-to-CO Conversion under Visible-Light Irradiation. *Molecules* **2019**, *24*, 1878−1890.
(27) Guillot, R.CSD Communication. 2021. CCDC 2078122.
(28) Martins, J. P.; Martín-Ramos, P.; Sobral, A. J. F. N.; Ramos-Silva, M. 4,7-Diphenyl-1,10-phenanthroline methanol hemisolvate. *Acta Crystallogr. Sect. E* **2013**, *69*, o1018.
(29) Wang, Y.; Jia, A.; Chen, X.; Shi, H.; Zhang, Q. Hydrogen-bonded assemblies of two organically templated borates: syntheses and crystal structures of $[(1,10\text{-phen})(H_3BO_3)_2]$ and $[2\text{-EtpyH}][(B_5O_6(OH)_4]$. *Z. Naturforsch. B* **2015**, *70*, 467−473.
(30) Mukherjee, A.; Grobelny, P.; Thakur, T. S.; Desiraju, G. R. Polymorphs, Pseudopolymorphs, and Co-Crystals of Orcinol: Exploring the Structural Landscape with High Throughput Crystallography. *Crys. Growth Des.* **2011**, *11*, 2637−2653.
(31) Chen, Z.; Zhang, Y.; Liang, F. Ethylenediammonium dichloride bis(1,10-phenanthroline) tetrahydrate. *Acta Crystallogr. Sect E* **2006**, *62*, o2797−o2799.
(32) Jones, C. L.; Milburn, G. H.; Sayer, L.; Hughes, D. L. Structure of the complex formed between ammonium picrate and 1,10-phenanthroline. *Acta Crystallogr. B* **1981**, *37*, 1548−1553.
(33) Dulz, G.; Sutin, P. N. The Kinetics of the Oxidation of Iron(II) and its Substituted im-(l,10-Phenanthroline) Complexes by Cerium-(IV). *Inorg. Chem.* **1963**, *2*, 917−921.
(34) Labanowski, J. K.; Andzelm, J. W.*Density Functional Methods in Chemistry*; Springer-Verlag: 1991.

https://doi.org/10.1021/acs.jpca.2c05879
J. Phys. Chem. A 2022, 126, 7261−7272

(35) Austin, A.; Petersson, G.; Frisch, M. J.; Dobek, F. J.; Scalmani, G.; Throssell, K. A density functional with spherical atom dispersion terms. *J. Chem. Theory and Comput.* **2012**, *8*, 4989−5007.
(36) Buhl, M.; Kabrede, H. Geometries of transition-metal complexes from Density-Functional Theory. *J. Chem. Theory Comput.* **2006**, *2*, 1282−1290.
(37) Jacobsen, H.; Cavallo, L. On the accuracy of DFT methods in reproducing ligand substitution energies for transition metal complexes in solution: The role of dispersive interactions. *ChemPhysChem* **2012**, *13*, 562−569.
(38) Ghosh, A. Just how good is DFT? *J. Biol. Inorg. Chem.* **2006**, *11*, 671−673.
(39) Harvey, J. N. On the Accuracy of Density Functional Theory in Transition Metal Chemistry. *Annual Reports Section C (Physical Chemistry)* **2006**, *102*, 203−226.
(40) Cramer, C. J.; Truhlar, D. G. Density functional theory for transition metals and transition metal chemistry. *Phys. Chem. Chem. Phys.* **2009**, *11*, 10757−10816.
(41) Krishnan, R.; Binkley, J. S.; Seeger, R.; Pople, J. A. Self-Consistent Molecular Orbital Methods. 20. Basis set for correlated wave-functions. *J. Chem. Phys.* **1980**, *72*, 650−654.
(42) Frisch, M. J.; Pople, J. A.; Binkley, J. S. Self-Consistent Molecular Orbital Methods. 25. Supplementary Functions for Gaussian Basis Sets. *J. Chem. Phys.* **1984**, *80*, 3265−3269.
(43) McLean, A. D.; Chandler, G. S. Contracted Gaussian-basis sets for molecular calculations. 1. 2nd row atoms, Z = 11−18. *J. Chem. Phys.* **1980**, *72*, 5639−5648.
(44) Wachters, A. J. H. Gaussian basis set for molecular wavefunctions containing third-row atoms. *J. Chem. Phys.* **1970**, *52*, 1033−1036.
(45) Hay, P. J. Gaussian basis sets for molecular calculations. The representation of 3d orbitals in transition metal atoms. *J. Chem. Phys.* **1977**, *66*, 4377−4384.
(46) Marenich, A. V.; Cramer, C. J.; Truhlar, D. G. Universal solvation model based on solute electron density and a continuum model of the solvent defined by the bulk dielectric constant and atomic surface tensions. *J. Phys. Chem. B* **2009**, *113*, 6378−96.
(47) Coyle, S.; Glaser, R. Asymmetric Imine *N*-Inversion in 3-Methyl-4-Pyrimidinimine. Molecular Dipole Analysis of Solvation Effects. *J. Org. Chem.* **2011**, *76*, 3987−3996.
(48) Frisch, M. J.; Trucks, G. W.; Schlegel, H. B.; Scuseria, G. E.; Robb, M. A.; Cheeseman, J. R.; Scalmani, G.; Barone, V.; Petersson, G. A.; Nakatsuji, H.; et al.*Gaussian 16*, Rev. C.01; Gaussian, Inc.: Wallingford, CT, 2016.
(49) Konig, E. Some aspects of the chemistry of bis(2,2'-dipyridyl) and bis(1,10-phenanthroline) complexes of iron(II). *Coord. Chem. Rev.* **1968**, *3*, 471−495.
(50) Burger, K.; Ebel, H.; Madeja, K. The effect of spin states of iron(II) on the XPS of its mixed complexes. *J. Electron. Spectrosc.* **1982**, *28*, 115−121.
(51) Goodwin, H. Spin transitions in six-coordinate iron(II) complexes. *Coord. Chem. Rev.* **1976**, *18*, 293−325.
(52) Yang, Y.; Zhang, X.; Zhong, L.; Lan, J.; Li, X.; Li, C.; Chung, L. W. Unusual KIE and dynamics effects in the Fe-catalyzed hetero-Diels-Alder reaction of unactivated aldehydes and dienes. *Nat. Commun.* **2020**, *11*, 1850−1860.
(53) Reinhard, M. E.; Mara, M. W.; Kroll, T.; Lim, H.; Hadt, R. G.; Alonso-Mori, R.; Chollet, M.; Glownia, J. M.; Nelson, S.; Sokaras, D.; et al. Short-lived metal-centered excited state initiates iron-methionine photodissociation in ferrous cytochrome c. *Nat. Commun.* **2021**, *12*, 1086−1094.
(54) Miessler, G. L.; Tarr, D. A.*Inorganic Chemistry*, 3rd ed.; Pearson: 2004.
(55) Glaser, R.; Choy, G. S.; Chen, G. S.; Grützmacher, H. Inductive and Conjugative S→C Polarizations in "Trithiocarbenium Ions" $[C(SH)_3]^+$ and $[C(SH)_3]^{\bullet,2+}$. Potential Energy Surface Analysis, Electronic Structure Motif, and Spin Density Distribution. *J. Am. Chem. Soc.* **1996**, *118*, 11617−11628.
(56) Glaser, R.; Chen, G. S.; Grützmacher, H. Effects of electron correlation and spin projection on rotational barriers of trithiocarbenium ion $[C(SH)_3]^+$ and Radical Dication $[C(SH)_3]^{\bullet,2+}$. *J. Comput. Chem.* **1997**, *18*, 1023−1035.
(57) Glaser, R.; Camasta, C. Electronic Structures and Spin Density Distributions of BrO_2 and $(HO)_2BrO$ Radicals. Mechanisms for Avoidance of Hypervalency and for Spin Delocalization and Spin Polarization. *Inorg. Chem.* **2013**, *52*, 11806−11820.
(58) Hammond, G. A. A Correlation of reaction rates. *J. Am. Chem. Soc.* **1955**, *77* (2), 334−338.
(59) Farcasiu, D. The Use and Misuse of the Hammond Postulate. *J. Chem. Educ.* **1975**, *52*, 76−79.
(60) Hunter, E. P. L.; Lias, S. Evaluated gas phase basicities and proton affinities of molecules: An update. *J. Phys. Chem. Ref. Data.* **1998**, *27*, 413−656.
(61) Burgot, J. New point of view on the meaning and on the values of $K_a(H_3O^+, H_2O)$ and $K_b(H_2O, OH^-)$ pairs in water. *Analyst* **1998**, *123*, 409−410.
(62) Shriver, D. F.; Atkins, P. W.*Inorganic Chemistry*, 3rd ed.; W. H. Freeman and Co.: 1999.

https://doi.org/10.1021/acs.jpca.2c05879
J. Phys. Chem. A 2022, 126, 7261−7272